Crystal Structure and Stability Studies of C77S HiPIP: A Serine Ligated [4Fe-4S] Cluster†

Sheref S. Mansy,[#] Yong Xiong,[‡] Craig Hemann,[§] Russ Hille,[§] M. Sundaralingam,*[,‡] and J. A. Cowan*[,#]

Evans Laboratory of Chemistry, Ohio State University, 100 West 18th Avenue, Columbus, Ohio 43210, Department of Molecular and Cellular Biochemistry, Ohio State University, 1645 Neil Avenue, Columbus, Ohio 43210, and Departments of Chemistry and Biochemistry, Macromolecular Structure Center, Ohio State University, 1060 Carmack Road, Columbus, Ohio 43210

Received September 18, 2001; Revised Manuscript Received November 7, 2001

ABSTRACT: The crystal structure of *Chromatium vinosum* C77S HiPIP has been determined and is compared with that of wild type. This is the first reported crystal structure of a Ser ligated [4Fe-4S] cluster and reveals a 0.11 Å shortening of the Fe−O bond (relative to Fe−S), but only minor structural alterations of the overall tertiary structure. Coordination changes are corroborated by resonance Raman spectroscopy. Comparison of the crystal and solution structures for HiPIPs identifies Phe48 as the main controller of solvent access to the Fe−S cluster; however, there is no significant change in cluster solvation of the C77S mutant relative to WT HiPIP. Ser ligation ultimately results in decreased cluster stability due to increased sensitivity to proton mediated degradation.

HiPIPs[1] are small $[4Fe\text{-}4S]^{3+/2+}$ cluster-containing proteins that are thought to be involved in electron-transfer reactions in photosynthetic bacteria. In some species, HiPIPs can act as an electron donor to the photosynthetic reaction center, interacting via surface hydrophobic patches (*1*). HiPIPs display a unique range of positive reduction potential of +50 to +450 mV (*2*), whereas those from low potential [4Fe-4S] proteins are in the range of −100 to −650 mV (*3*). Much effort has been expended on efforts to alter the reduction potential of HiPIPs by introduction of point mutations at residue sites defining the hydrophobic core surrounding the [4Fe-4S] cluster. However, rather than perturbing the reduction potential significantly, these mutations had the effect of decreasing cluster stability, and so the aromatic side-chains surrounding the cluster appear to protect the [4Fe-4S] cluster from hydrolytic attack rather than to modulate reduction potential (*3*−*5*). Such considerations have also led to investigations of cluster assembly and disassembly pathways (*6*−*8*) that are relevant in the context of iron sensing Fe−S proteins and mechanisms of cellular iron homeostasis (*9*).

The majority of known [4Fe-4S] proteins contain clusters coordinated by four cysteines. Aconitase provided the first example of noncysteinyl coordination, in which one of the ligands is a solvent oxygen (*10*). Other examples include Ni−Fe hydrogenase from *Desulfovibrio gigas* with a [4Fe-4S] cluster ligated by histidine (*11*), and *Pyrococcus furiosus* ferredoxin with a [4Fe-4S] cluster ligated by an aspartate (*12*). As in the case of aconitase, the oxygen ligated iron in *P. furiosus* ferredoxin can be lost thereby generating a [3Fe-4S] cluster (*13*, *14*).

Site-directed mutagenesis is now commonly applied to mutations of cluster-bound cysteines in an attempt to identify or alter the ligands to an Fe−S cluster. In some instances, it has been found that the isosteric serine can substitute for cysteine as an unnatural ligand to the cluster. However, due to the low success rate, decreased stability of the cluster, and lack of natural examples, it appears that cysteine is significantly favored over serine. Indeed, for *Azotobacter vinelandii* ferredoxin I, protein rearrangement resulting in remote cysteinyl ligation is preferred over coordination to a serine substituted in place of a ligating cysteine (*15*). Although there are no examples of natural serine coordination to canonical Fe−S clusters, serine has been identified as a ligand to the molybdenum center of dimethyl sulfoxide reductase (*16*), and a serine of the oxidized nitrogenase molybdenum−iron protein P-cluster may serve an auxiliary role by providing additional coordination to one of the iron atoms (*17*).

The X-ray crystal structures of two classes of Fe−S protein have previously been reported following the introduction of a Cys to Ser ligand change, including the $Fe(Cys)_4$ rubredoxin center and a [2Fe-2S] cluster (*18*, *19*). However, no such examples exist for a [4Fe-4S] cluster. Relative to wild type (WT) protein, it has been previously shown that C77S HiPIP coordinates a less stable [4Fe-4S] cluster that is ligated by the O_γ of Ser77 and is accompanied by no gross structural perturbations (*20*, *21*). Although the NMR solution structure of C77S HiPIP has been solved (*21*), a detailed comparison between WT and C77S HiPIP clusters and the details of

† This work was supported by a grant from the Petroleum Research Fund, administered by the American Chemical Society (J.A.C.), the National Science Foundation, CHE-0111161 (J.A.C.), the NIH grant GM-59953 (R.H.), and the NIH Grant GM-17378 (M.S.). S.S.M. was supported by the NIH Chemistry and Biology Interface Training Program at Ohio State University (GM08512-03).

* Address correspondence to Professor J. A. Cowan at the Department of Chemistry, Ohio State University, 100 West 18th Ave., Columbus, OH 43210. E-mail: cowan@chemistry.ohio-state.edu; tel: 614 292 2703, fax: 614 292 2703.

[#] Evans Laboratory of Chemistry.

[‡] Departments of Chemistry and Biochemistry.

[§] Department of Molecular and Cellular Biochemistry.

[1] Abbreviations: CCD, charge-coupled device; HiPIP, high potential iron protein; NMR, nuclear magnetic resonance; Tris, tris(hydroxymethyl)-aminomethane; WT, wild type.

10.1021/bi011811y CCC: $22.00
Published on Web 12/29/2001

cluster coordination was precluded as a result of the paramagnetism of the cluster. X-ray crystallography can provide additional and more accurate structural details of the cluster environment. Here we report the first X-ray crystal structure of a serine oxygen ligated [4Fe-4S] cluster. Comparisons of the cluster and surrounding aromatic residues of *Chromatium vinosum* C77S HiPIP and WT HiPIP are discussed.

MATERIALS AND METHODS

Protein Purification and Crystallization. Preparation and initial purification procedures were as previously described (*20*, *22*). Further purification was achieved by gel filtration (G-75, Pharmacia) with 10 mM Tris-HCl, pH 8.0, as the running buffer. C77S HiPIP was concentrated via ultrafiltration (Amicon) to 1.1 mM. Hollow rectangular rod shaped crystals with typical dimensions of 0.05 × 0.05 × 0.5 mm grew within 4 days in the dark at room temperature via the hanging drop technique. Protein (2 μL) was mixed with an equal volume of reservoir solution [45.5% (v/v) saturated ammonium sulfate and 49.8 mM KCl] and 2 μL of 50% 2-methyl-2, 4-pentanediol and allowed to equilibrate with 1 mL of reservoir solution via vapor diffusion.

Crystal Data Collection. Crystal data was collected at 100 K at beam line 14 BM-C of the Advanced Photon Source (APS) at Argonne National Labs. The crystals were transferred to the reservoir solution supplemented with 6% glycerol and immediately frozen inside a loop prior to data collection. Extensive attempts of freezing the crystal as the whole hollow rod were unsuccessful due to its fragility. Therefore, one wall of the hollow rod was cut into a 0.01 × 0.02 × 0.04 mm piece and subsequently used for data collection. This piece of crystal diffracted to 1.9 Å resolution. The crystal was indexed in the monoclinic space group $P2_1$ with cell constants $a = 67.06$ Å, $b = 30.18$ Å, $c = 68.74$ Å, and $\beta = 111.27°$. The cell volume indicated that there were four independent protein molecules in the asymmetric unit. Crystal data were processed with DENZO and SCALEPACK (*23*).

Structure Solution and Refinement. The structure was solved by the molecular replacement method using the program AmoRe (*24*). H42Q HiPIP (*9*) was used as the search model. The model was refined to 1.9 Å using the program CNS (*25*). The crystallized C77S HiPIP contains five additional amino acid residues at the amino-terminus not found in native HiPIP or in the model (*22*). These additional residues were fitted to the electron density according to its known sequence (*22*). A total of 188 water molecules were added for the four independent molecules. The final R/R-free is 19.3%/23.4% in the resolution range of 15−1.9 Å. The crystal data, and structure refinement statistics are shown in Table 1. The coordinates have been deposited in the Protein Data Bank (PDB) with accession code 1JS2.

Resonance Raman Spectroscopy. Protein concentrations were 3.7 mM WT HiPIP and 3.3 mM C77S HiPIP in 10 mM Tris-HCl, pH 8.0. Oxidized samples were prepared by the addition of a 10-fold molar excess of $K_3Fe(CN)_6$, incubation on ice for 5 min, and desalting via a short G-25 (Pharmacia) column, and then immediately frozen on dry ice until further use.

Table 1: Crystal Data and Refinement Statistics

space group:	$P2_1$	
cell parameters:	$a = 67.06$ Å	$\alpha = 90°$
	$b = 30.18$ Å	$\beta = 111.27°$
	$c = 68.74$ Å	$\gamma = 90°$
no. of protein molecules in a.u.:	4	
wavelength:	1.653 Å	
resolution:	1.9 Å	
unique reflections:[a]	35 617	
completeness (%):	90.4	
Rsym (%):	9.4	
refinement (15 Å−1.9 Å):		
R-work/R-free:	23.4/19.3	
protein atoms:	2672	
water molecules	188	
rmsd bonds:	0.010	
rmsd angles:	1.3	

[a] Friedel pairs unmerged.

Resonance Raman spectra were obtained with a Chromex 500IS single-stage 0.5-m imaging spectrograph equipped with an 1800 groove/mm grating. The detector was a Princeton Instruments, Inc. LN/CCD-1024TKB liquid nitrogen cooled, 1024 × 1024 pixel array, back-thinned, charge-coupled device (CCD). All excitation lines were generated by a Coherent INNOVA 307 Ar^+ ion laser. Scattered photons were collected at 180° from a frozen sample (approximately 35 μL) placed in the sample well of a nickel plated sample holder affixed to the coldfinger of an APD Cryogenics Inc. Displex DE-204SL two-stage, closed cycle helium refrigerator held at 30 K by a Lakeshore 330 Autotuning Temperature Controller. Rayleigh scattering was rejected by using a holographic notch filter (Kaiser Optical Systems, Inc.) that was angle tuned for maximum spectral coverage. The detector control software used was the CCD Spectrometric Multichannel Analysis (CSMA) software version 2.2a provided by Princeton Instruments, Inc. Spectra were calibrated using a software package based on the ASYST scientific software package (Asyst Software Technologies) and further developed in the laboratory of Dr. Terry Gustafson at The Ohio State University. Indene, frozen in one of the three sample wells, was used for calibration. A quadratic fit to the indene Raman bands served as the calibration function for converting from pixel number on the CCD to wavenumber shift. Raman band center frequencies were determined using the PEAKFIT program (Jandel Scientific) running on a PC/DOS platform.

Cluster Stability. A 100 mM buffered protein solution in a 1.0-cm path-length cuvette was repeatedly degassed under vacuum and purged with argon. Buffers were pH 10.0 CAPS, pH 7.0 sodium phosphate, and sodium citrate at pH 4.0 and 3.0. Reactions were initiated at room temperature by the addition of argon-purged HiPIP to a concentration of 35 μM and monitored by the decrease of cluster absorbance at 386 nm on a Hewlett-Packard 8425A diode array spectrophotometer using the On-Line Instrument Systems (OLIS) 4300S Operating System software.

RESULTS

Protein Conformation and [4Fe-4S] Cluster Coordination. The association of the four independent molecules in the asymmetric unit is shown in Figure 1. In agreement with previous NMR results, the overall tertiary structure of C77S

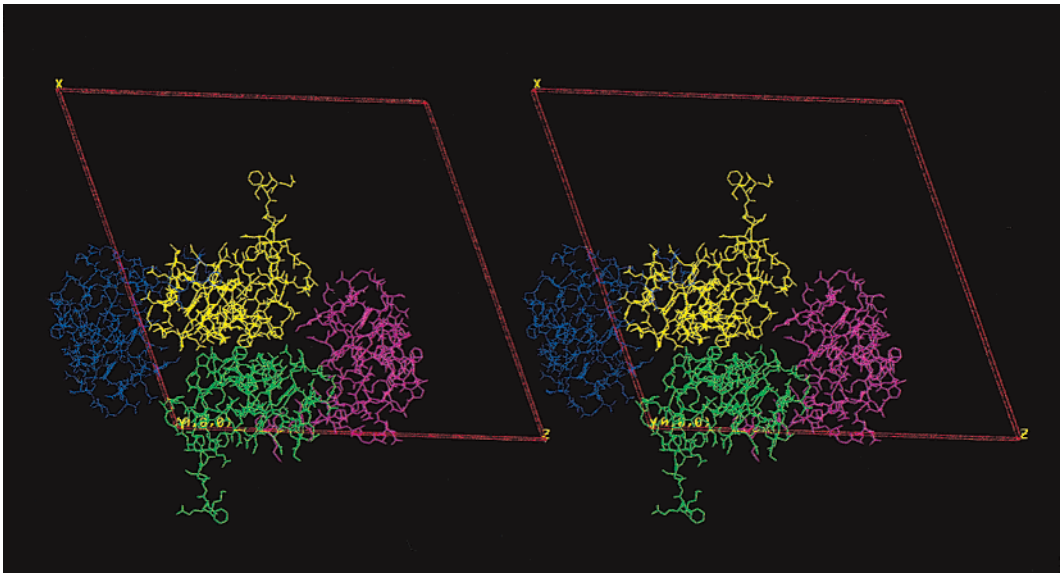

FIGURE 1: The association of the four independent molecules in the asymmetric unit.

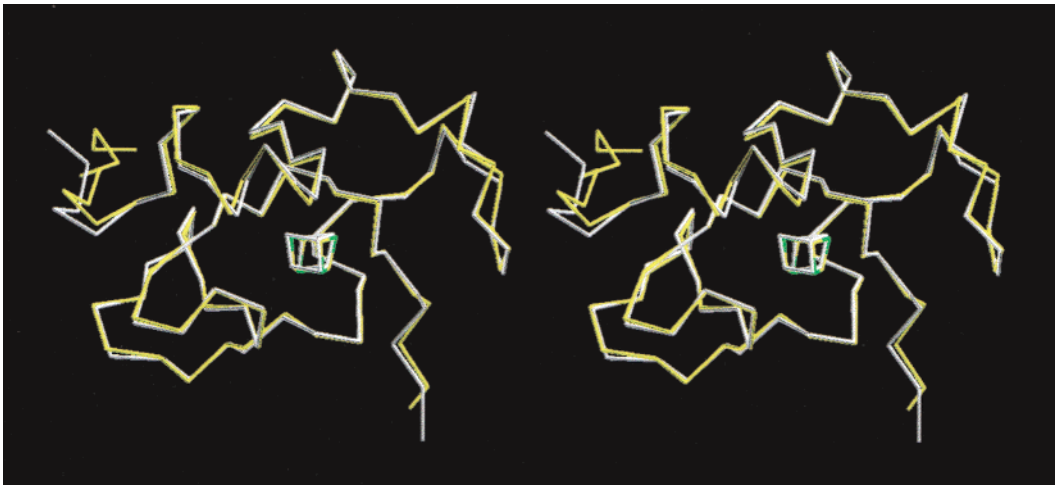

FIGURE 2: Superposition of the C_α backbones of C77S (yellow) and WT (white) HiPIP.

HiPIP was essentially unaltered when compared with WT (*21*) with a rmsd of 0.89 Å (Figure 2). Moreover, the [4Fe-4S] cluster itself was remarkably similar to the WT cluster (Table 2). Although the differences between the mean cluster interatomic distances for WT and C77S HiPIP are within experimental error, a trend of shorter Fe−inorganic sulfide (S*) bond lengths associated with the Ser ligated Fe (Fe4) is apparent. The [4Fe-4S] cluster protein ligands of C77S HiPIP were not greatly perturbed. However, there was a noticeable lengthening of the preserved Cys−Fe bonds, and a shortening of the Ser77−Fe bond (Table 2 and Figure 3), indicating a slight migration of the [4Fe-4S] cluster toward the introduced oxygen ligand. Three of the four C77S HiPIP molecules within the asymmetric unit had Ser77−Fe4 distances between 2.10 and 2.14 Å with the fourth molecule having a distance of 2.27 Å. Nevertheless, the mean Ser77−Fe4 distance was 0.11 Å shorter than the Cys77−Fe4 distance found for WT HiPIP. It is also worth noting that no attempts were made to maintain the reduced state of the crystal during data acquisition. However, the conditions used were identical to that for the HiPIP structures reported by Parisini et al. (*26*) and are unlikely to result in oxidation at 100 K. Therefore, good comparisons between WT and C77S HiPIP structures can be made and are supported by resonance Raman results discussed below.

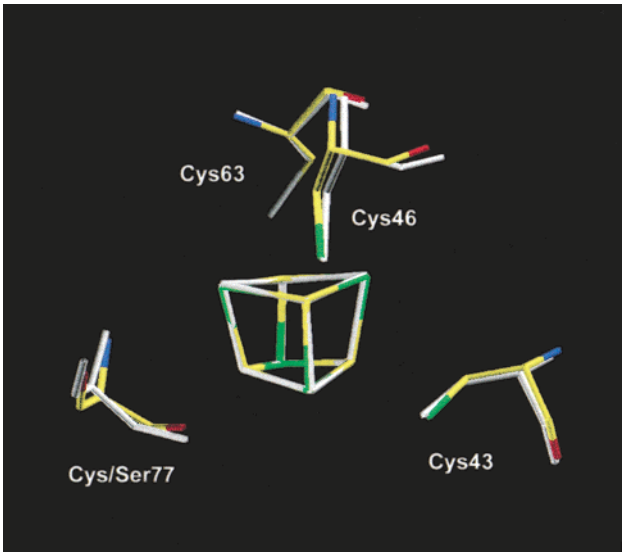

FIGURE 3: C77S and WT HiPIP cluster and cluster ligands. The superposition of C77S (colored) and WT (white) HiPIP were centered on the [4Fe-4S] cluster.

Table 2: Comparison between C77S and WT HiPIP Mean Fe−S Cluster Bond Lengths and Dihedral Angles

	WT[a]	C77S[b]	difference[c]
Fe−S* Distances, Å			
Fe1−S*2	2.31	2.29	−0.02
Fe2−S*1	2.30	2.30	0.00
Fe3−S*3	2.32	2.31	−0.01
Fe4−S*4	2.28	2.18	−0.10
mean	2.30	2.27	−0.03
Fe1−S*1	2.33	2.32	−0.01
Fe2−S*2	2.31	2.31	0.00
Fe3−S*4	2.32	2.30	−0.02
Fe4−S*3	2.30	2.19	−0.11
mean	2.32	2.28	−0.04
Fe1−S*3	2.24	2.26	0.02
Fe2−S*4	2.22	2.27	0.05
Fe3−S*2	2.25	2.18	−0.07
Fe4−S*1	2.28	2.20	−0.08
mean	2.25	2.23	−0.02
Fe−Protein Ligand (S_γ/O_γ) Bond Distances, Å			
Cys43−Fe1	2.26	2.33	+0.07
Cys46−Fe2	2.30	2.36	+0.06
Cys63−Fe3	2.27	2.36	+0.09
Cys/Ser77−Fe4	2.27	2.16	−0.11
Fe−(S_γ/O_γ)−C_β−C_α Dihedral Angles, deg			
Cys43	−67	−62	+5
Cys46	−173	−171	+3
Cys63	127	125	−2
Cys/Ser77	−79	−99	−20
Hydrogen Bond Distances, Å			
N48−S_γ46	3.45	3.45	0.00
N81−S_γ46	3.67	3.51	−0.16
N65−S_γ63	3.30	3.26	−0.04
N79−(S_γ/O_γ)77	3.37	3.17	−0.20
N49−S*2	3.82	3.78	−0.04
N77−S*1	3.41	3.43	+0.02

[a] Taken from Parisini et al. (*26*). [b] Present work. [c] Positive and negative numbers indicate an increase and decrease, respectively, for C77S relative to WT HiPIP. Standard deviations are less than 0.01 for Fe−S* bond distances, less than 0.05 for Fe-protein ligand bond distances (except for Ser77-Fe4, 0.08), less than 4 for dihedral angles, and less than 0.11 for hydrogen bond distances (except for N81−S_γ46, 0.16).

The Aromatic Core Surrounding the [4Fe-4S] Cluster. The residues defining the aromatic hydrophobic core are Tyr19, Phe48, Phe66, Trp76, and Trp80. In particular, Tyr19 has been implicated in maintaining cluster stability due to its close proximity to the cluster (*27*). We have found only slight differences in Tyr19 positioning with respect to the cluster (Figure 4). The Tyr19 C_δ1-S*3 and C_δ1-(S/O_γ)77 distances for C77S HiPIP are 3.71 and 5.29 Å, respectively, and are 3.69 and 5.41 Å, respectively, for WT HiPIP. Furthermore, Trp76 and Trp80 remain relatively unchanged. Banci et al. noted an altered Phe66 orientation between crystal and solution structures of WT HiPIP (*28*). We also observe a slightly altered Phe66 orientation (Phe66 tilts 29.6° in the C77S HiPIP structure). However, the most dramatic difference observed in the C77S HiPIP structure is the rearrangement of Phe48, which is tilted 34.5° toward S*46 (Figure 4).

Backbone Amide Hydrogen Bonds and Water Content of C77S HiPIP. None of the backbone amide to cysteinyl-S or S* hydrogen bonds were disrupted in the C77S HiPIP structure (Table 2). These hydrogen bonds have been suggested to stabilize the structure as well as to modulate the reduction potential of HiPIP (*29*). All of the [4Fe-4S] cluster associated hydrogen bond distances were essentially

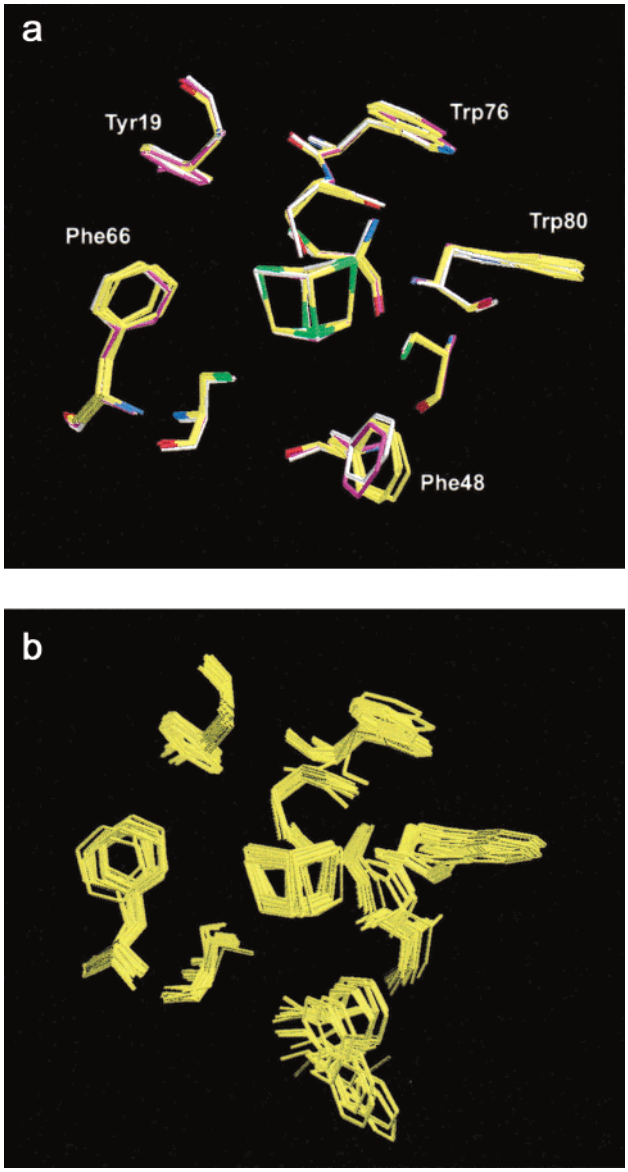

FIGURE 4: Comparison of C77S and WT HiPIP cluster, cluster ligands, and surrounding hydrophobic residues after superimposing their C_α backbones. (a) Crystal structures of C77S HiPIP (yellow), WT HiPIP (white, *26*), H42Q HiPIP (magenta, *26*). (b) Solution structures of WT HiPIP (*28*).

unaltered except for N81−S_γ46 and N79−(S_γ/O_γ)77. A similar deviation for the N81−S_γ46 hydrogen bond was observed for H42Q HiPIP and therefore does not seem to be a manifestation of an altered Fe−S ligand. The shortening of the N79−(S_γ/O_γ)77 hydrogen bond is expected due to the greater electronegativity of an oxygen atom.

As previously noted, the major consideration with regards to cluster stability is solvent accessibility to the cluster. Of the three conserved water positions noted by Parisini et al. (*26*), none were found to be significantly altered in the C77S HiPIP structure. Therefore, neither increased solvent accessibility to the cluster nor disruption of stabilizing hydrogen bonds can be used as an explanation for the decreased stability of the C77S HiPIP mutant.

Resonance Raman Spectroscopy. Raman spectroscopy is a sensitive technique to characterize metal coordination to biological molecules (*30*, *31*). A comparison of the resonance Raman spectra of C77S and WT HiPIP in both the reduced

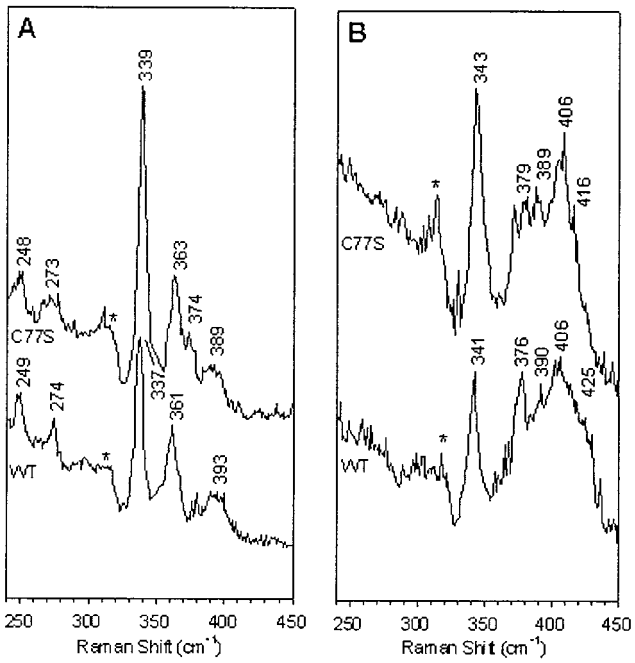

FIGURE 5: Resonance Raman spectra of C77S and WT HiPIPs in (A) the reduced and (B) oxidized states. All spectra were recorded on frozen samples at 30 K using an excitation wavelength of 488 nm and a laser power of approximately 120 mW. The spectrograph was set with an 1800 groove/mm holograph grating and a 50 μm input slit width for each spectrum. The (*) denotes bands due to frozen solvent.

Table 3: Resonance Raman Frequencies for C77S and WT HIPIPs[a]

WT, reduced	C77S, reduced	WT, oxidized	C77S, oxidized
Mainly Terminal Fe−S Stretching Modes			
393	389	406	406
361	363	376	379
Mainly Bridging Fe−S Stretching Modes			
		390	389
337	339	341	343
274	273		
249	248		

[a] All frequencies are in cm^{-1}.

and oxidized states are illustrated in Figure 5. Important spectral features are compared in Table 3. Consistent with previous studies (*32*, *33*), there was an upshift of the totally symmetric vibration of the [4Fe-4S] core [$A_1{}^b$ mode where b refers to a bridging mode (*33*)] upon oxidation for both C77S and WT HiPIP. This upshift was 4 cm^{-1} for both forms of HiPIP (from 339 to 343 cm^{-1} for C77S and from 337 to 341 cm^{-1} for WT HiPIP), which compares favorably with the 3−5 cm^{-1} upshifts reported previously for WT (*32*, *33*). At both oxidation states, the cluster's totally symmetric vibration upshifted by 2 cm^{-1} for C77S relative to WT HiPIP. Above 340 cm^{-1}, the resonance Raman spectrum of reduced WT HiPIP was dominated by the asymmetric Fe−S(Cys) mode at 361 cm^{-1} and a broad, less intense band centered at 393 cm^{-1} in the proper energy range for a symmetric Fe−S(Cys) mode. Minor alterations within this region were observed for C77S HiPIP and are further discussed below (see Discussion). No band was observed in the range 550−650 cm^{-1} that might be attributed to Fe−O bonding.

C77S HiPIP Cluster Acid Sensitivity. Both WT and C77S HiPIPs were quite stable at basic pH showing no signs of cluster degradation after 1 h at room temperature

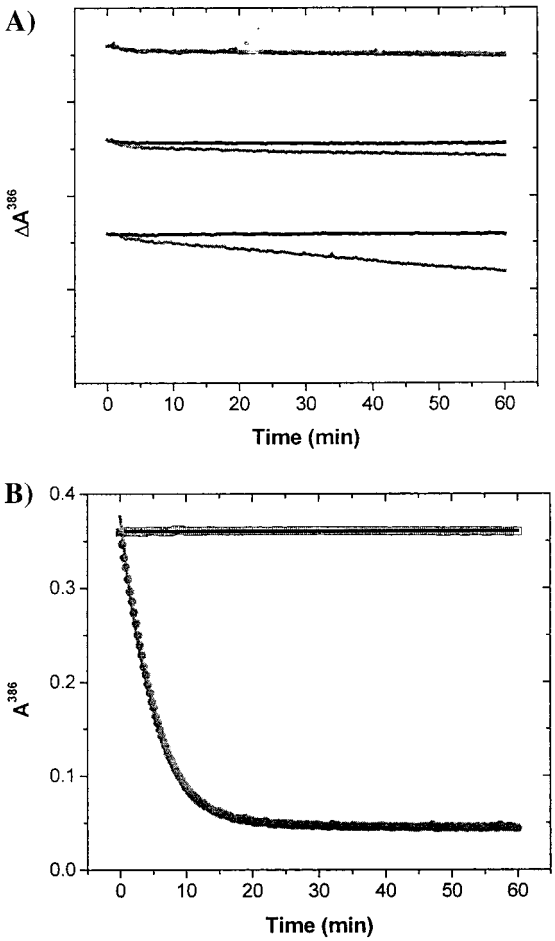

FIGURE 6: Acid catalyzed [4Fe-4S] degradation. (A) Cluster degradation of C77S (gray) and WT (black) HiPIP at pH 10.0 (top lines), pH 7.0 (middle lines), and pH 4.0 (bottom lines). Each tick mark on the *y*-axis represents a change in absorbance at 386 nm of 0.5. (B) Cluster degradation at pH 3.0. Data were fit to a first-order exponential decay.

(Figure 6). WT HiPIP continued to remain stable at all pHs tested. However, under more acidic conditions the C77S HiPIP cluster began to degrade. At pH 3.0, the cluster of C77S HiPIP rapidly degraded with a $t_{1/2}$ of 4 min.

DISCUSSION

The shortening of the Ser77−Fe4 bond by 0.11 Å is significantly less than that observed for *Anabaena* C49S ferredoxin (0.3 Å) (*19*) and *C. pasteurianum* C42S rubredoxin (0.4 Å) (*18*). The reasons for this are unclear. C42S rubredoxin loses a Cys42(S_γ)−N44 hydrogen bond upon Ser substitution, which may facilitate the lengthening of the Ser42−Fe bond. However, C49S ferredoxin retains all of its cluster-associated hydrogen bonds. A more likely explanation is the rigidity of the polypeptide backbone. EXAFS results of single Cys to Ser mutants of rubredoxin suggests that interior ligand mutants have Ser−Fe bond lengths more similar to WT than exterior ligand mutants (C42 is an exterior ligand, i.e., more solvent exposed) (*18*). Such findings are consistent with greater backbone rigidity maintaining a particular ligand−Fe bond length. NMR studies have shown that HiPIP retains its structural integrity in the presence of 3 M guanidinium hydrochloride and only partially unfolds in 3.3 to 4.4 M guanidinium hydrochloride (*34*). Furthermore,

the [4Fe-4S] cluster of HiPIP is deeply buried within its hydrophobic core (*35*). Thus, the conservation of protein ligand−Fe bond lengths for C77S HiPIP is likely a consequence of its great structural rigidity and its ability to surround the [4Fe-4S] cluster with hydrophobic residues.

Resonance Raman spectra of C77S and WT HiPIP revealed slight differences in cluster coordination. In particular, the increase in energy of the $A_1{}^b$ mode upon oxidation has been attributed to an overall shortening of the Fe−S* bonds of the cluster (*32*). Interestingly, this same mode was shifted 2 cm^{-1} higher in the C77S mutant form of HiPIP relative to WT in both oxidation states. This is consistent with the crystallographic data that revealed a minor shortening of the Fe−S* bond lengths in the C77S mutant relative to WT reduced HiPIPs. This upshift in the $A_1{}^b$ mode was also reported in a study of four serine variants of *P. furiosus* ferredoxin (*14*). Relative to the complete cysteinyl-ligated mutant form of *P. furiosus* ferredoxin (D14C), the upshifts of this mode ranged from 2 to 5 cm^{-1} for single Cys to Ser variants. Resonance Raman spectra could not be acquired for all of the individual Cys to Ser cluster ligands of *C. vinosum* HiPIP due to cluster instability (*20*).

In the study of the serine variants of *P. furiosus* ferredoxin (*14*), the asymmetric Fe−S(Cys) modes proved most sensitive to changes in cluster ligation with the general trend being downshifts of varying degree for both the symmetric and asymmetric $Fe-S^t$ (t denotes terminal protein−ligand modes) modes relative to the system with complete cysteinyl ligation. Our data compare very closely with that of the D14S *P. furiosus* ferredoxin mutant in which the symmetric $Fe-S^t$ mode shifted down by 3 cm^{-1} from 395 cm^{-1} in the D14C mutant to 392 cm^{-1}, the asymmetric $Fe-S^t$ mode shifts down 1 cm^{-1} from 363 to 362 cm^{-1}, and the $A_1{}^b$ mode mentioned above shifts up by only 2 cm^{-1}. The other serine mutants in this study showed much larger shifts in one or more of these modes. In the present study, relative to reduced WT HiPIP, these same modes in the reduced C77S mutant HiPIP resonance Raman spectrum shifted by −4, +2, and +2 cm^{-1}. These minor shifts reflect the subtle changes seen in the crystallographic data for reduced C77S HiPIP in which the $Fe-S_g$ bonds elongated by less than 0.1 Å and the $Fe-S_g-C_b-C_a$ dihedral angles changed by less than 5 degrees relative to WT (Table 2).

Comparisons of all of the *C. vinosum* HiPIP crystal structures solved to date are nearly identical with the largest significant discrepancy being the positioning of Phe48. Even within our single crystal the Phe48 orientation differs among the four molecules of the asymmetric unit. An analysis of the accepted NMR structures of WT and C77S HiPIP reveals even greater heterogeneity for Phe48 positioning (*21*, *28*). Thus, a unique situation exists in which the flexibility of a side-chain can be corroborated both by crystal and solution structures of a protein. Such flexibility at this location within HiPIP is particularly significant since Phe48 protects the cluster from its most solvent-exposed region, which is consistent with NMR studies that identify Phe48 as being crucial in maintaining solvent exclusion from the cluster (*36*). Therefore, the normal breathing of the molecule may ultimately result in Phe48 controlling solvent access to the cluster by alternating between "open" and "closed" conformations similar to that of the distal histidine of hemoglobin which controls ligand entry into the heme pocket via a swinging gate mechanism (*37*). Phe66 orientation is also altered between the different HiPIP structures, although to a much lesser extent than for Phe48. Phe66 flexibility may be indicative of a less frequently available solvent path to the cluster, or a manifestation of its ability to accommodate structural changes such as those encountered upon the "opening" of Phe48 and subsequent solvent entry. Surprisingly, a comparison of solved HiPIP structures from different bacteria reveals that neither Phe48 nor Phe66 are absolutely conserved. An analysis of their structures indicates that those HiPIPs with analogous Phe48 and Phe66 residues, such as *Ectothiorhodospira halophila* HiPIP (*38*), more likely go through a cluster degradation pathway similar to that described for *C. vinosum* HiPIP. However, those with a nonconserved Phe48, as in *Ectothiorhodospira vacuolata* HiPIP (*39*−*41*), or nonconserved Phe48 and Phe66 positions, as in *Rhodocyclus tenuis* HiPIP (*42*), appear to have different faces of the Fe−S cluster that are maximally exposed to solvent and therefore may have different routes for solvent entry.

The reasons for the decreased cluster stability of C77S HiPIP are not readily apparent from the crystal structure. Neither cluster geometry, protein backbone or side-chain orientations, water positioning, nor hydrogen bonding to the cluster are significantly perturbed. Therefore, there must be other nonstructural factors associated with the intrinsic properties of Fe−S coordination by a serine ligand that make such interactions less favorable. All Cys to Ser mutations of Fe−S cluster ligating residues reported in the literature thus far have resulted in decreased cluster stability. Our observation of increased cluster susceptibility to acid-catalyzed degradation is consistent with the findings of Wedd and colleagues (*18*). Xiao et al. noted complete loss of Fe coordination to all single Cys to Ser mutants of *C. pasteurianum* rubredoxin within 5 min under acidic conditions, whereas native rubredoxin required at least an hour under the same conditions (*18*). Such differences in stability can be attributed to the much greater difficulty in maintaining a deprotonated serine rather than a cysteine. For a simple Fe−S cluster as in rubredoxin, which contains no inorganic sulfides, the mechanism of acid catalyzed cluster disassembly is not significantly perturbed inasmuch as both mutant and native cluster degradation pathways most likely initiate with the protonation of protein ligand side-chains, although the order of ligand protonation may be altered. However, for a more complex Fe−S cluster as found in HiPIP the mechanism by which the cluster degrades is likely to be more significantly affected. The initial steps of the HiPIP [4Fe-4S] acid-catalyzed cluster degradation pathway are thought to initiate by protonation of the bridging inorganic sulfides, not the protein ligands (*43*). Thus, the introduction of an easily protonated protein ligand allows for an altered and more facile route to the loss of Fe−S coordination.

Often Cys to Ser mutant Fe−S proteins express in the apoform (*44*). Indeed, Fe−S coordination is a necessary step in the proper folding of HiPIP (*6*). Therefore, interference with the formation of the appropriate Fe−S(Cys) bonds may result in an inability of the protein to attain its functional conformation (*6*, *9*). Mutations of cysteines that initiate cluster formation would be expected to result in a greater decrease in in vivo and in vitro formation of holo-protein than mutations of residues that coordinate to the cluster in the final stages of assembly. This again can be readily

explained by a comparison of the pK_a values of cysteine and serine. The energetic penalty for deprotonating a serine (pK_a ~ 16) is much greater than that for deprotonating a cysteine (pK_a ~ 8.35) (*18*, *45*, *46*). Such an effect would be particularly dominating in the early stages of cluster assembly since the protein has not yet had the opportunity to create an interior cluster-coordinating cavity, which could potentially alter the pK_a of the subsequent ligating residues, thus making bond formation more favorable.

CONCLUSIONS

We have determined the crystal structure and report the results for the first Ser ligated [4Fe-4S] protein, thus confirming the presence of the Ser(O_γ)−Fe bond. Ser ligation effectively preserves the overall geometry and bond lengths of the HiPIP protein and Fe−S cluster. The major effect of Ser ligation appears to be sensitivity to proton mediated cluster disassembly, as a result of the increased pK_a for Ser relative to Cys, rather than from structural factors. Furthermore, Phe48 has been identified as a likely candidate for the control of solvent access to the Fe−S cluster.

ACKNOWLEDGMENT

We thank Jon-David Sears and Don Ordaz of the OSU Fermentation facility for help with bacterial fermentations. We thank APS and Argonne National Laboratory for supporting the synchrotron data collection.

REFERENCES

1. Nogi, T., Fathir, I., Kobayashi, M., Nozawa, T., and Miki, K. (2000) *Proc. Natl. Acad. Sci. U.S.A. 97*, 13561−13566.
2. Bartsch, R. G. (1978) *Methods Enzymol. 53*, 329−340.
3. Cowan, J. A., and Lui, S. M. (1998) *Adv. Inorg. Chem. 45*, 313−350.
4. Iwagami, S. G., Creagh, A. L., Haynes, C. A., Borsari, M., Felli, I. C., Piccioli, M., and Eltis, L. D. (1995) *Protein Sci. 4*, 2562−2572.
5. Bertini, I., Borsari, M., Bosi, M., Eltis, L. D., Felli, I. C., Luchinat, C., and Piccioli, M. (1996) *J. Biol. Inorg. Chem. 1*, 257−263.
6. Natarajan, K., and Cowan, J. A. (1997) *J. Am. Chem. Soc. 119*, 4082−4083.
7. Bian, S., and Cowan, J. A. (1998) *J. Am. Chem. Soc. 120*, 3532−3533.
8. Bian, S., Cowan, J. A. (1999) *Coordination Chem. Rev. 190*−*192*, 1049−1066.
9. Bentrop, D., Bertini, I., Iacoviello, R., Luchinat, C., Niikura, Y., Piccioli, M., Presenti, C., and Rosato, A. (1999) *Biochemistry 38*, 4669−4680.
10. Robbins, A. H., and Stout, C. D. (1989) *Proc. Natl. Acad. Sci. U.S.A. 86*, 3639−3643.
11. Volbeda, A., Charon, M.-H., Piras, C., Hatchikian, E. C., Frey, M., and Fontecilla-Camps, J. C. (1995) *Nature 373*, 580−587.
12. Calzolai, L., Gorst, C. M., Zhao, Z.-H., Teng, Q., Adams, M. W. W., and La Mar, G. N. (1995) *Biochemistry 34*, 11373−11384.
13. Beinert, H., and Thomson, A. J. (1983) *Arch. Biochem. Biophys. 222*, 333−361.
14. Brereton, P. S., Duderstadt, R. E., Staples, C. R., Johnson, M. K., and Adams, M. W. W. (1999) *Biochemistry 38*, 10594−10605.
15. Shen, B., Jollie, D. R., Diller, T. C., Stout, C. D., Stephens, P. J., and Burgess, B. K. (1995) *Proc. Natl. Acad. Sci. U.S.A. 92*, 10064−10068.
16. Schindelin, H., Kisker, C., Hilton, K. J., Rajagopalan, K. V., and Rees, D. C. (1996) *Science 272*, 1615−1621.
17. Kim, J., and Rees, D. C. (1992) *Science 257*, 1677−1682.
18. Xiao, Z., Lavery, M. J., Ayhan, M., Scrofani, S. D. B., Wilce, M. C. J., Guss, J. M., Tregloan, P. A., George, G. N., and Wedd, A. G. (1998) *J. Am. Chem. Soc. 120*, 4135−4150.
19. Hurley, J. K., Wever-Main, A. M., Hodges, A. E., Stankovich, M. T., Benning, M. M., Holden, H. M., Cheng, H., Xia, B., Markley, J. L., Genzor, C., Gomez-Moreno, C., H., R., and Tollin, G. (1997) *Biochemistry 36*, 15109−15117.
20. Agarwal, A., Li, D. L., and Cowan, J. A. (1996) *J. Am. Chem. Soc. 118*, 927−928.
21. Bentrop, D., Bertini, I., Capozzi, F., Dikiy, A., Eltis, L., and Luchinat, C. (1996) *Biochemistry 35*, 5928−5936.
22. Agarwal, A., Tan, J., Eren, M., Tevelev, A., Lui, S. M., and Cowan, J. A. (1993) *Biochem. Biophys. Res. Commun. 197*, 1357.
23. Otwinowski, Z., and Minor, W. (1997) *Methods Enzymol. 276*, 307−326.
24. Navaza, J. (1994) *Acta Crystallogr. A50*, 157−163.
25. Brunger, A. T., Adams, P. D., Clore, G. M., DeLano, W. L., Gros, P., Grosse, Kunstleve, R. W., Jinag, J., Kuszewski, J., Nilges, M., Pannu, N. S., Read, R. J., Rice, L. M., Simonson, T., and Warren, G. L. (1998) *Acta Cryst. D54*, 905−921.
26. Parisini, E., Capozzi, F., Lubini, P., Lamzin, V., Luchinat, C., and Sheldrick, G. M. (1999) *Acta Crystallogr. D55*, 1773−1784.
27. Agarwal, A., Li, D. L., and Cowan, J. A. (1995) *Proc. Natl. Acad. Sci. U.S.A. 92*, 9440−9444.
28. Banci, L., Bertini, I., Dikiy, A., Kastrau, D. H. W, Luchinat, C., and Sompornpisut, P. (1995) *Biochemistry 34*, 206−219.
29. Carter, C. W. (1977) in *Iron*−*Sulfur Proteins* (Lovenberg, W., Ed.) pp 157−204, Academic Press, New York.
30. Long, T. V., and Loehr, T. M. (1970) *J. Am. Chem. Soc. 92*, 6384−6386.
31. Mansy, S., Wood, T. E., Sprowles, J. C., and Tobias, R. S. (1974) *J. Am. Chem. Soc. 96*, 1762−1770.
32. Backes, G., Mino, Y., Loehr, T. M., Meyer, T. E., Cusanovich, M. A., Sweeney, W. V., Adman, E. T., and Sanders-Loehr, J. (1991) *J. Am. Chem. Soc. 113*, 2055−2064.
33. Czernuszewicz, R. S., Macor, K. A., Johnson, M. K., Gewirth, A., and Spiro, T. G. (1987) *J. Am. Chem. Soc. 109*, 7178−7187.
34. Bertini, I., Cowan, J. A., Luchinat, C., Natarajan, K., and Piccioli, M. (1997) *Biochemistry 36*, 9332−9339.
35. Carter, C. W., Kraut, J., Freer, S., Xuong, N.-H., Alden, R. A., and Bartsch, R. G. (1974) *J. Biol. Chem. 249*, 4212−4225.
36. Soriano, A., and Cowan, J. A. (1996) *Inorg. Chim. Acta 251*, 285−290.
37. Perutz, M. F., and Mathews, F. S. (1966) *J. Mol. Biol. 21*, 199−202.
38. Breiter, D. R., Meyer, T. E., Rayment, I., and Holden, H. M. (1991) *J. Biol. Chem. 266*, 18660−18667.
39. Benning, M. M., Meyer, T. E., Rayment, I., and Holden, H. M. (1994) *Biochemistry 33*, 2476−2483.
40. Banci, L., Bertini, I., Eltis, L. D., Felli, I. C., Kastrau, D. H. W., Luchinat, C., Piccioli, M., Pierattelli, R., and Smith, M. (1994) *Eur. J. Biochem. 225*, 715−725.
41. Bertini, I., Couture, M. J., Donaire, A., Eltis, L. D., Felli, I. C., Luchinat, C., Picciolo, M., and Rosato, A. (1996) *Eur. J. Biochem. 241*, 440−452.
42. Rayment, I., Wesenber, G., Meyer, T. E., Cusanovich, M. A., and Holden, H. M. (1992) *J. Mol. Biol. 228*, 672−686.
43. Foster, M. W., Bian, S., Surerus, K. K., and Cowan, J. A. (2001) *J. Biol. Inorg. Chem. 6*, 266−274.
44. Moulis, J.-M., Davasse, V., Golinelli, M.-P., Meyer, J., and Quinkal, I. (1996) *J. Biol. Inorg. Chem. 1*, 2−14.
45. Xia, B., Cheng, H., Bandarian, V., Reed, G. H., and Markley, J. L. (1996) *Biochemistry 35*, 9488−9495.
46. Cowan, J. A. (1997) *Inorganic Biochemistry: An Introduction*, 2nd ed., Wiley-VCH, Inc, New York.

BI011811Y